Active OB stars: structure, evolution, mass loss, and critical limits
Proceedings IAU Symposium No. 272, 2010
C. Neiner, G. Wade, G. Meynet & G. Peters, eds.

doi:10.1017/S1743921311009963

Interferometric studies of rapid rotators

Ming Zhao[1], John D. Monnier[2] and Xiao Che[2]

[1]Jet Propulsion Laboratory, 4800 Oak Grove Dr, Pasadena, CA 91101
email: ming.zhao@jpl.nasa.gov

[2]Dept. of Astronomy, University of Michigan, 500 Church St., Ann Arbor, MI 48109

Abstract. Stellar rotation, like stellar mass and metallicity, is a fundamental property of stars. Rapid rotation distorts the stellar photosphere and affects a star's luminosity, abundances and evolution. It is also linked to stellar wind and mass loss. The distortion of the stellar photosphere due to rapid rotation causes the stellar surface brightness and effective temperature to vary with latitude, leading to a bright pole and a dark equator - a phenomenon known as 'Gravity Darkening'. Thanks to the development of long baseline optical interferometry in recent years, optical interferometers have resolved the elongation of rapidly rotating stars, and have even imaged a few systems for the first time, directly confirming the gravity darkening effect. In this paper, we review the recent interferometric studies of rapid rotators, particularly the imaging results from CHARA-MIRC. These sub-milliarcsecond resolution observations permit the determination of the inclination, the polar and equatorial radius and temperature, as well as the fractional rotation speed of several rapid rotators with unprecedented precision. The modeling also allows the determination of the true effective temperatures and luminosities of these stars, permitting the investigation of their true locations on the HR diagram. Discrepancies from standard models were also found in some measurements, suggesting the requirement of more sophisticated mechanisms such as non-uniform rotation in the model. These observations have demonstrated that optical interferometry is now sufficiently mature to provide valuable constraints and even model-independent images to shed light on the basic physics of stars.

Keywords. stars: fundamental parameters, stars: rotation, stars: imaging, techniques: interferometric

1. Introduction

Stellar rotation, like stellar mass and metallicity, is a fundamental property of stars. For decades, stellar rotation was generally overlooked in stellar models and was regarded to have a trivial influence on stellar evolution because most stars are slow rotators, such as the Sun (Maeder & Meynet 2000). Although the effects of rotation on solar type stars are indeed relatively mild, they are more prominent on hot stars. Studies have shown that a large fraction of hot stars are rapid rotators with rotational velocities more than 120 km s^{-1} (Abt & Morrell 1995; Abt *et al.* 2002). Virtually all the emission-line B (Be) stars are rapid rotators with rotational velocities of $\sim$ 90% of breakup (Frémat *et al.* 2005). Rapid rotation affects stellar brightness distribution, internal flows, stellar evolution, and circumstellar environments (Maeder & Meynet 2000) - almost all aspects of stellar astrophysics.

Traditionally, stellar rotation is studied using spectra line profiles, doppler imaging, photometry and polarimetry. Techniques such as asteroseismology also become popular in recent years (e.g., Gizon & Solanki 2004). These methods are all very powerful in characterizing stellar structure and/or rotation. On the other hand, they also have constraints and sometimes even require good knowledge of the targets. For instance, Vega shows narrow lines typical of slow rotation (Vsini$\sim$21 km s^{-1}). However, some weak metal spectra lines are "flat-bottomed" (Gulliver *et al.* 1994). The "flat-bottomed" line

profiles have led to inaccurate determination of its inclination angle (Hill *et al.* 2004) until Vega was confirmed to be a pole-on rapid rotator by interferometry (Peterson *et al.* 2006; Aufdenberg *et al.* 2006), and rotation-induced macro turbulence of 7-10 km s^{-1} was included in the model (Yoon *et al.* 2008; Hill *et al.* 2010). This suggests that detailed studies of stars require measurements from multiple techniques to provide multi-angle views and disentangle degeneracies of parameters.

In the past few years, optical interferometers have resolved the elongated photospheres of rapidly rotating stars for the first time. More excitingly, interferometric observations have lead to the first images of main sequence stars other than the Sun, showing the elongated photospheres and uneven surface brightness distributions due to rapid rotation. The emergence of these high angular resolution observations of hot stars has shined a spotlight on critical areas of stellar evolution and basic astrophysics that demand our attention. Measurements from interferometers can determine the oblateness, geometry, rotational speed, and surface brightness distribution of rapid rotators, and even provide model-independent images of stars. These measurements can directly and independently provide constraints to other measurements such as spectroscopy and asteroseismology, providing better understanding of the structure and physics of the targets. In this paper, we review the recent interferometric studies of rapid rotators, particularly the imaging results from CHARA-MIRC.

The paper is organized as follows. We briefly discuss the effects of rapid rotation in §2, and give a minimal overview of the basics of interferometry in §3. We highlight the recent interferometric studies in §5 and present some CHARA imaging results in §6. Finally, we give some future prospects in §7.

2. Effects of rapid rotation

Stars that are rapidly rotating have many unique characteristics. The centrifugal force from rapid rotation distorts their photospheres and causes them to be oblate. In the standard Roche approximation (i.e., point mass distribution and uniform rotation), the maximum equatorial to polar radius ratio due to the rotational distortion has a maximum value of 1.5. Recent studies also suggest that this ratio can be larger than 1.5 with quadrupolar moment and/or differential rotation (Zahn *et al.* 2010; MacGregor *et al.* 2007).

The distortion of stellar surface also causes the surface brightness and the effective temperature (T_{eff}) to vary with latitude, and the equatorial temperatures are predicted to be much cooler than their polar temperatures, a phenomenon known as "Gravity Darkening" (von Zeipel 1924a,b). The standard gravity darkening law suggests $T_{eff} \propto g^{\beta}$, where g is the local gravity and β is the gravity darkening coefficient (von Zeipel 1924a). β equals to 0.25 for stars with radiative envelopes (von Zeipel 1924a), while it equals to 0.08 for stars with convective envelopes (Lucy 1967). For stars in the transition stage between radiative and convective envelopes, the value of β can be in between (Claret 2003).

Large rotation can modify the interior angular momentum of stars, causing internal flows and even differential rotation (e.g., Jackson *et al.* 2004). Recent stellar models show that rapid rotation can also cause abundance anomalies by rotation-induced mixing (Pinsonneault 1997). Rapid rotation also affects stellar luminosity and evolution, and increase stellar lifetime, which can cause scatters to the H-R diagram and may even alter the Mass-Luminosity relation (Maeder & Meynet 2000). In addition, stellar rotation can affect circumstellar environments through enhanced stellar winds and mass loss (e.g.,

Maeder *et al.* 2007), and it is even linked to Gamma-Ray bursts (MacFadyen *et al.* 2001; Burrows *et al.* 2007). A more detailed review can be found in Maeder & Meynet (2000).

3. Basics of interferometric studies

3.1. *Interferometric observables*

Interferometers combine light from distant objects using multiple telescopes and measure the interference of light. The light collected by telescopes is combined to form interference fringes similar to those of the Young's Double Slit experiment. The fringe contrast (also known as the fringe visibility, V) along with the associated phase are then measured by detectors. These two quantities together, also known as the complex visibility, are the basic observables in interferometry.

The visibility amplitude (i.e., the fringe contrast mentioned above) measures the angular scale of a target along the projected direction of a telescope-pair on the sky. The angular resolution is determined by the projected baseline between the two telescopes by $\lambda/2B_{proj}$, where λ denotes the wavelength and B_{proj} denotes the projected baseline. A point source gives unit visibility, while a resolved source gives much lower visibility. Therefore, by measuring a target along different directions on the sky, we can determine its shape and know if it is larger in one direction than the other.

Phase is another important quantity in the complex visibility as it carries information about the brightness distribution of the source. However, the phase of the light wave coming from a distant source is always corrupted as atmospheric turbulence always induces random and extra phase shifts. This makes the phases of complex visibilities useless. Nevertheless, we can combine 3 telescopes in a closed triangle, and the extra phase seen by each telescope can be canceled in a closed form (see Monnier 2003, for details). This phase closure, or closure phase, carries some intrinsic phase information of the target. It is immune to any phase shifts induced by the atmosphere and many other systematic errors as well. Because of this, it was widely applied to very long baseline interferometry in radio to compensate poor phase stability (Monnier 2003). Closure phase is also a good quantity for stable and precise measurements, and is widely used in aperture synthesis imaging for phase calibration (e.g., Zhao *et al.* 2008).

In addition, differential phase is another widely used quantity in interferometry. It measure the phase difference at two wavelengths, and therefore can also eliminate the phase error caused by atmospheric turbulence. Differential phase is sensitive to chromatic signatures and shift of photo-centers of the targets due to e.g., star spots, non-radial pulsations, and rotation, etc. (see e.g., Jankov *et al.* 2001)

3.2. *Interferometric Imaging*

Using visibilities and closure phases, one can construct models for a stellar object. A model-independent image on the other hand, is more intuitive and can provide more straightforward information.

According to the van Cittert-Zernike theorem (see e.g., Thompson *et al.* 1986), the complex visibility of an object is directly linked to the Fourier transform of its intensity distribution. Thus, the intensity distribution can be inverted by the inverse Fourier transform of its complex visibilities. However, in reality this inversion process is not straightforward as the actual sampling of the complex visibility space is always sparse and discrete. One needs a reasonable number of samplings to get enough information of the original intensity distribution, and a large number of sample points can greatly help the reconstruction of the image. In ground-based interferometry, this problem can be

slightly improved by the Earth's rotation, as the baselines' projected directions change while the Earth rotates, providing more samplings of the visibility space.

Because of the limited visibility and phase information, special imaging algorithms are thus required for image reconstruction. The reconstruction generally has many possible solutions. Thus some reasonable constraints are applied to regulate the solution, for instance, limiting the field-of-view of the image, making the imaging as smooth as possible, and providing a *priori* information to constrain the image.

Popular image reconstruction algorithms include CLEAN (Högbom 1974), the Maximum Entropy Method (MEM) (Narayan & Nityananda 1986), and the Markov Chain Monte-Carlo imaging (MCMC) (e.g., Ireland *et al.* 2006), etc. CLEAN is widely used in radio interferometry, while MEM and MCMC is more commonly adopted in optical/IR interferometry. Other imaging algorithms such as MIRA (Thiébaut 2008) are also emerging and can produce robust reconstructions. More details of optical interferometric imaging can be found in Malbet *et al.* (2010); Cotton *et al.* (2008) and references therein. All the images we present in §6 are reconstructed using the MACIM package, and details can be found in Ireland *et al.* (2006).

4. Modeling of rapid rotators

Here we briefly introduce the standard Roche - von Zeipel model commonly used in interferometry for rapid rotators. The basic assumptions of the Roche model (Cranmer & Owocki 1995) are point mass concentrated in the center of star and uniform rotation. These assumptions, together with the von Zeipel's theorem (see §2), allow us to construct a 2-dimensional map of a rapid rotator with six parameters: the stellar radius and temperature at the pole (R_{pol}, T_{pol}), the angular rotation rate as a fraction of breakup (ω), the gravity darkening coefficient β, the inclination angle i, and the position angle (east of north) ϕ of the star. The detailed prescription of the model can be found in Cranmer & Owocki (1995) and Aufdenberg *et al.* (2006).

Similar prescriptions can also be found in other literatures such as Domiciano de Souza (2009). The constructed 2D sphere is then projected onto the sky according to the position angle ϕ, and the inclination i. The intensity and limb darkening at each point of the stellar surface is calculated using stellar atmosphere models such as the Kurucz models (Kurucz 1993) and the PHOENIX models (Aufdenberg *et al.* 2006) as a function of local effective temperature, gravity, viewing angle, and wavelength.

5. Highlights of early observations

The development of long baseline optical interferometry in recent years has provoked many observations on nearby rapid rotators since the first observation in 2001 (van Belle *et al.* 2001). We highlight some of the results below.

Altair. Altair (α Aquilae, A7IV-V, HR 7557, $V = 0.77$, $H = 0.102$) was the first rapid rotator observed by interferometer (van Belle *et al.* 2001) . It is a member of the famous "Summer Triangle" (the other two stars are Vega and Deneb). Altair shows very large projected velocity, varying from 200 km s^{-1} to 242 km s^{-1} (e.g., Abt & Morrell 1995). Using the Palomar Testbed Interferometer (PTI), van Belle *et al.* (2001) found that Altair is elongated and one dimension is $\sim 14\%$ larger than the other (see the left panel of Fig. 1). Using NPOI, Ohishi *et al.* (2004) found that Altair has asymmetric surface brightness distribution and its pole is brighter than other parts of the star. Using the same data, Peterson *et al.* (2006) and Domiciano de Souza *et al.* (2005) independently

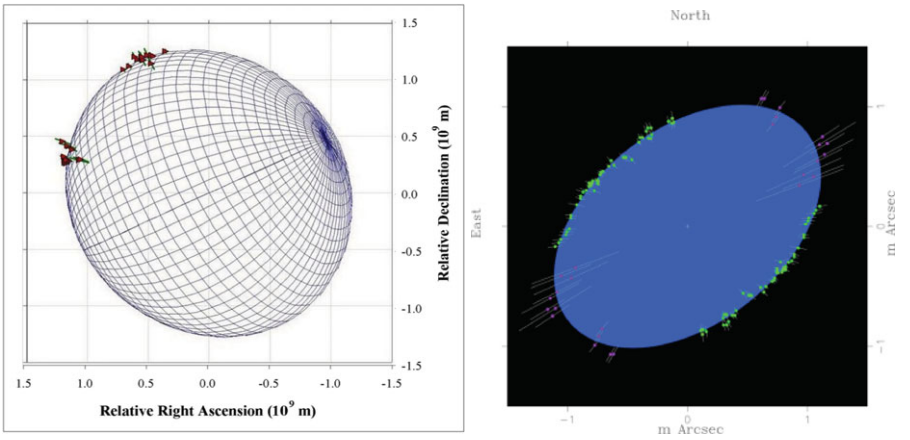

Figure 1. *Left*: PTI measurements of Altair (van Belle *et al.* 2001). The orientation of the star was flipped by 180^o in the original paper and is corrected in this plot (van Belle 2009, private communication). The red triangles show the measured sizes of Altair at different directions. *Right*: VLTI/VINCI measurements of Achernar (Domiciano de Souza *et al.* 2003). The colored dots show the angular diameter measurements along the stellar surface, indicating the star is strongly elongated.

modeled Altair using the gravity darkening model and confirmed the oblateness and asymmetric structure of Altair due to rapid rotation.

Regulus. Regulus (α Leo, HR3982, V = 1.35, H = 1.658) is a B7V (Johnson & Morgan 1953) or B8 IVn (Gray *et al.* 2003) star in a triple system. The rapid rotation of the primary was first measured by McAlister *et al.* (2005) with the CHARA array in the K' band. Combining the visibilities with spectroscopic measurements, McAlister *et al.* (2005) found Regulus is seen nearly equator-on, and its photosphere is very elongated due to rapid rotation, with an R_{eq}/R_{pol} ratio of 1.32. Recently, Gies *et al.* (2008) discovered that the primary is also a spectroscopic binary with a white dwarf company.

Achernar. The most extreme case of rapid rotation known to date comes from the brightest Be star Achernar (α Eri, HR 472, V=0.50, H =0.865). Using the VINCI instrument at the Very Large Telescope Interferometer (VLTI), Domiciano de Souza *et al.* (2003) measured the rotational flattening of Achernar to have a R_{eq}/R_{pol} ratio of 1.56 (left panel of Fig. 1), significantly higher than the limit given by the Roche approximation (1.5). This deviation suggests the basic assumption of Roche approximation may not be valid in this type of stars and differential rotation may exist (e.g., Jackson *et al.* 2004). Recent studies also suggest that an equatorial circumstellar disk/envelope could exist and contribute partially to the observed large flattening of Achernar (Vinicius *et al.* 2006; Kanaan *et al.* 2008). In addition, Kervella & Domiciano de Souza (2006) also found strong polar emission that can account for $\sim 5\%$ of the near-IR flux of Achernar. These discoveries have made Achernar an extreme and ideal test case for theoretical models, and have evoked extensive discussions in the field.

Vega. Perhaps the most compelling results of rapid rotators come from the photometric standard Vega (α Lyr, HR 7001, A0V). For decades, Vega was found to be anomalously brighter than the average A0V stars by 0.5 mag in V (Millward & Walker 1985). Early interferometric studies ruled out the binary hypothesis and also found that Vega's radius is significantly larger (60% larger) than that of Sirius, a A1V star. These phenomenon implied that Vega may be a rapid rotator seen pole-on. The flat-bottomed appearance of some weak metal lines of Vega, in addition, also suggests the same hypothesis.

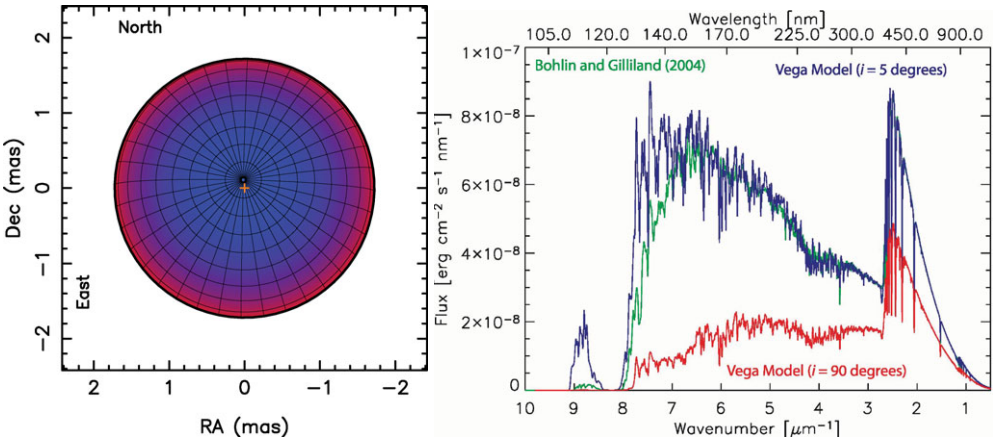

Figure 2. *Left*: Gravity darkening model of Vega from Peterson *et al.* (2006) using NPOI, showing that Vega is a nearly pole-on star. *Right*: The SED model of Vega, seen at the pole ($i = 5^o$, blue) and the equator ($i = 90^o$, red) respectively (Aufdenberg *et al.* 2006). The SEDs at the polar and the equatorial regions are significantly different due to the large temperature differences.

The mystery was eventually uncovered by interferometric measurements from both the CHARA array (Aufdenberg *et al.* 2006) and the Navy Prototype Optical Interferometer (NPOI) (Peterson *et al.* 2006). By measuring the extra darkening at the stellar limbs caused by gravity darkening (Aufdenberg *et al.* 2006) and the closure phase (Peterson *et al.* 2006) respectively, these two studies both confirmed that Vega is indeed a nearly pole-on rapid rotator ($i \sim 5^o$) rotating at $\sim 91\% - 93\%$ of its angular break-up rate (Fig. 2). They also show that the polar radii of Vega is over 23% shorter than that of the equator, while the temperature at the poles is over 2000K hotter than that of the equator.

6. Imaging of rapid rotators

The interferometric studies mentioned above have confirmed the oblateness of rapid rotators and the general picture of von Zeipel's gravity darkening law for the first time, greatly improved our understandings of rapid rotators. On the other hand, discrepancies with the basic assumptions such as solid rotation and point mass distribution of stars are also raised. Indeed, more sophisticated hydrodynamical models have shown that non-solid body rotation such as differential rotation and meridional flows can exist in these stars (e.g., Jackson *et al.* 2004; MacGregor *et al.* 2007). To shed light on these issues, and further advance our knowledge of the physics of rapid rotation, "model-independent" images are necessary to test wide variety of models and to provide more intuitive knowledge of those stars.

Most of the previous interferometric studies were entirely based on model-fitting of interferometric visibilities with a few baselines, and therefore are not able to generate model-independent images. However, thanks to the recent development of imaging combiners such as CHARA-MIRC (Monnier *et al.* 2004) and VLTI-AMBER (Petrov *et al.* 2007), imaging stellar surfaces with only a few milli-arcseconds across has become true.

Up to date, imaging studies of rapid rotators have been carried out for five stars (Altair, Alderamin, Rasalhague, Regulus, Caph) and four of them have been successfully imaged. All of the images were obtained with CHARA-MIRC at the near-IR H band. Below we highlight the results from these studies.

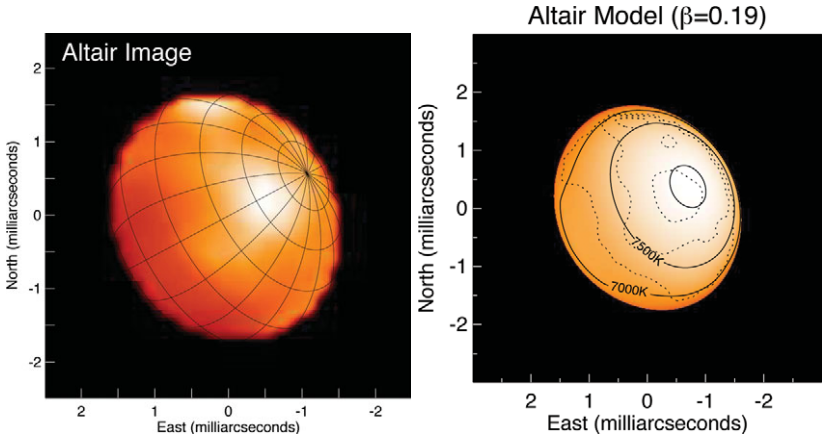

Figure 3. Reconstructed image of Altair and comparison with its gravity darkening model (Monnier *et al.* 2007). The angular resolution is $\sim$ 0.64 milliarcseconds. The latitudes and longitudes are overplotted to show the geometry of the star (left). The bright feature in the upper-most limb of the star is artifact that is beyond the resolution limit. The right panel shows the gravity darkening model for Altair, with the temperature contours from both the model (solid lines) and the image (dotted lines). The brightest spot of the stellar surface is shifted slightly to the center because of limb darkening and the fact the pole of Altair is seen at the limb.

Altair. The first image was obtained for Altair by Monnier *et al.* (2007). The left panel of Fig. 3 shows the reconstructed image. The image shows that the stellar photosphere of Altair is well-resolved and appears oblate, with a bright polar area and dark equatorial area - directly confirming the gravity darkening phenomenon. The right panel of Fig. 3 shows the gravity darkening model of Altair fitted to compare with the image. The model shows Altair is medium inclined, with an inclination of 57^o and is rotating at 92.3% of its angular break-up rate. The temperature at the poles is 8450K, while that of the equator is only 6860K, suggesting the existence of convective equator and radiative poles. The model also prefers a non-standard β of 0.19. The contours of the model match with the image very well in general except at the equator where the image appears to be darker and colder.

Alderamin. The star Alderamin (α Cephei, HR 8162, V=2.46, H=2.13) was classified as an A7 IV-V star in early studies, and was recently classified as an A8V main sequence star by Gray *et al.* (2003). It is one of the few A stars (including Altair) that are found to have chromosphere activities (Walter *et al.* 1995; Simon *et al.* 2002). van Belle *et al.* (2006) studied Alderamin using the CHARA array and found it is rotating close to break-up and is elongated. Observations from Zhao *et al.* (2009) yielded an image of Alderamin and an improved model. As shown in Fig. 4, Alderamin is also elongated, with a bright pole at the bottom and a dark equator in the middle. The top of the image appears bright again due to the gravity darkening effect. The model of Alderamin suggests it is inclined by 56^o and is rotating at $\sim$92.6% of its angular break-up rate. The temperature at the poles is $\sim$2400 K higher than at the equator, while its radius at the equator is 26% larger than at the poles. The non-standard β value of 0.22, and the low temperature at the equator, plus the evidence of strong chromosphere activities directly linked to convection implies the equator of Alderamin is probably also convective. This similar feature of both Alderamin and Altair indicates that rapid rotators can have both radiative and convective envelopes and a clear boundary between convective stars and radiative stars may not exist.

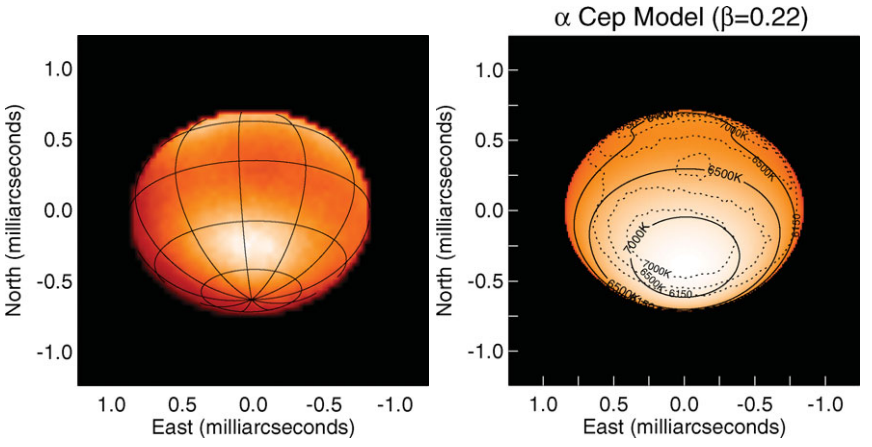

Figure 4. Reconstructed image of Alderamin and comparison with its gravity darkening model. The angular resolution is ~ 0.68 milliarcseconds. The latitudes and longitudes are overplotted to show the geometry of the star. The right panel shows the corresponding gravity darkening model for Alderamin, with the temperature contours from both the model (solid lines) and the image (dotted lines). (Zhao *et al.* 2009)

Rasalhague. Rasalhague (α Ophiuchi, HR 6556, $V = 2.09$, H=1.66) is a nearby subgiant binary system (Wagman 1946). The primary is a A5IV sub-giant (Gray *et al.* 2001). Several groups have tried to study the orbit of the system (e.g., Mason *et al.* 1999, etc.), and it was lately determined to have a period of ~ 8.6 yrs and a semi-major axis between 0.4" - 0.5".

Zhao *et al.* (2009) have tried extensively to reconstruct an image for Rasalhague but failed to find a reliable solution due to the fact it is seen nearly pole-on ($i = 88^o$), which makes the star nearly symmetric and thus hard to constrain by closure phases (closure phases are only sensitive to asymmetries). Figure 5 shows the model of Rasalhague. The right panel shows the degeneracy between β and the inclination angle which is also caused by the symmetric brightness distribution of Rasalhague. Fortunately, this degeneracy can be partially lifted with the aid of Vsini measurements, although the scatter of various measurements from literatures is large. The model shows that the photosphere of Rasalhague is also very elongated and has bright poles and a dark equator. Its radius at the equator is $\sim$20% larger than at the poles. It is rotating at 88.5% of its angular break-up speed and the poles are $\sim$1840 K hotter than the equator.

Regulus. Regulus was first studied by McAlister *et al.* (2005) with the CHARA array (see §5). We revisited Regulus with CHARA-MIRC and created an image along with a refined model for it (Che *et al.*, in preparation). The model is consistent with that of McAlister *et al.* (2005), showing that Regulus is also nearly equator-on ($i = 85.7^o$) and is rotating at a high angular rate of 95.3% of its breakup, causing its radius at the equator 29% larger than that of the poles. The temperature at pole is about 14300K, about 3000K hotter than that of the equator ($\sim$ 11260 K). As a late B type star with temperatures well above 11000K, Regulus should be radiative and β should be 0.25. However, our best-fit model still prefers a non-standard β of 0.18, implying that the standard von Zeipel's law may not be full-filled in this case and non-uniform rotation may exist in Regulus as well.

Caph. Caph (β Cassiopeiae, HR21, V = 2.27, H = 1.585) is a late type F2III-IV star that has evolved off the main sequence (Rhee *et al.* 2007). Its Vsini has been measured to be between 70 km s^{-1} to 83 km s^{-1}, relatively low compared to other rapid rotators. Our observations in 2007 and 2009 have also allowed us to reconstruct an image and

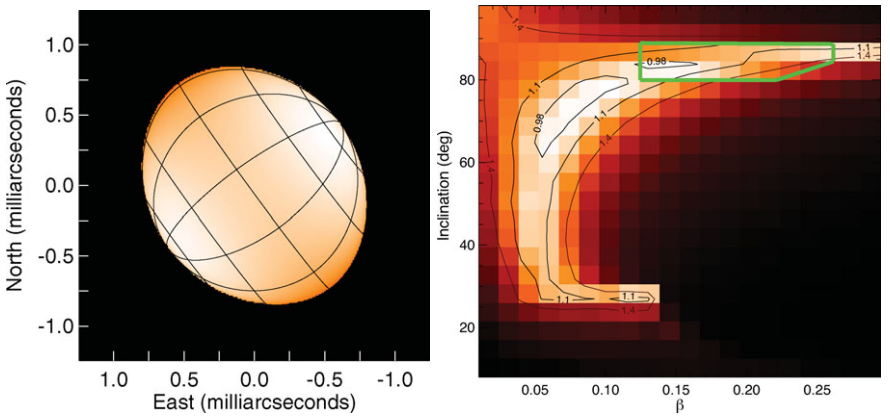

Figure 5. *Left*: The gravity darkening model of Rasalhague. *Right*: Reduced χ^2 space of inclination and β. The green box indicates the parameter space constrained with Vsini measurements.

model for it (Che *et al.*, in preparation). The results show that Caph is rotating at 93.6% of its angular breakup speed, and is seen nearly pole-on ($i = 18^o$) like Vega. Therefore, although its oblateness ratio is about 26%, its appearance on the sky is not elongated. Its polar temperature is only about 7200K and it has a β of about 0.15.

To summarize all the interferometric observations to date, we list the targets and their physical parameters in Table 1. The table shows that all the best-fit β values (Regulus, Altair, Alderamin, Caph) are lower than the standard of 0.25, suggesting the basic assumptions of the standard model may be hard to full-fill in most cases (even for some B type stars like Regulus), and non-uniform rotation is necessary to be included at this level to address the issue.

With the parameters from the gravity darkening models, we are able to calculate the true T_{eff}s and luminosities of these stars and compare with their apparent values. This also allows us to locate their true positions on the HR diagram. Figure 6 shows the HR diagram for four stars: Altair, Vega, Alderamin, and Rasalhague, and marks their apparent positions and true positions on the diagram. Non-rotation equivalents of these stars are also marked for comparison with non-rotating stellar evolution models. These figures suggest that the apparent position of a rapid rotator is strongly dependent on its inclination, i.e., the viewing angle. For a $\sim 90^o$ inclination star such as Rasalhague

Table 1. Summary of interferometric observations of rapid rotators (ranked by spectral type)

Star	**inclination** deg	$\mathbf{T}_{pol}$ K	$\mathbf{R}_{pol}$ $R_\odot$	$\mathbf{T}_{eq}$ K	$\mathbf{R}_{eq}$ $R_\odot$	ω %	β
Achernar[a]	50	20000	8.3	9500	12	-	0.25 (fixed)
Regulus[e]	85.7 ± 0.8	14315 ± 370	3.17 ± 0.03	11261 ± 170	4.08 ± 0.39	95.3 ± 1.2	0.178 ± 0.010
Vega[1,b]	4.7 ± 0.3	10150 ± 100	2.26 ± 0.07	7900 ± 400	2.78 ± 0.02	91 ± 3	0.25 (fixed)
Rasalhague[d]	87.7 ± 0.4	9300 ± 150	2.39 ± 0.01	7460 ± 100	2.87 ± 0.02	88.5 ± 1.1	0.25 (fixed)
Altair[c]	57.2 ± 1.9	8450 ± 140	1.63 ± 0.01	6860 ± 150	1.48 ± 0.01	92.3 ± 0.6	0.190 ± 0.012
Alderamin[d]	55.7 ± 6.2	8588 ± 300	2.16 ± 0.04	6574 ± 300	2.74 ± 0.04	94.1 ± 2.0	0.216 ± 0.021
Caph[e]	18.2 ± 3.8	7236 ± 111	2.99 ± 0.14	6058 ± 93	3.77 ± 0.17	93.6 ± 5.4	0.149 ± 0.017

References: *a*. Domiciano de Souza *et al.* (2003); *b*. Aufdenberg *et al.* (2006); *c*. Monnier *et al.* (2007); *d*. Zhao *et al.* (2009); *e*. Che *et al.*, in preparation
[1]**Note**: Peterson *et al.* (2006) have also determined consistent physical parameters for Vega, and thus are not listed here.

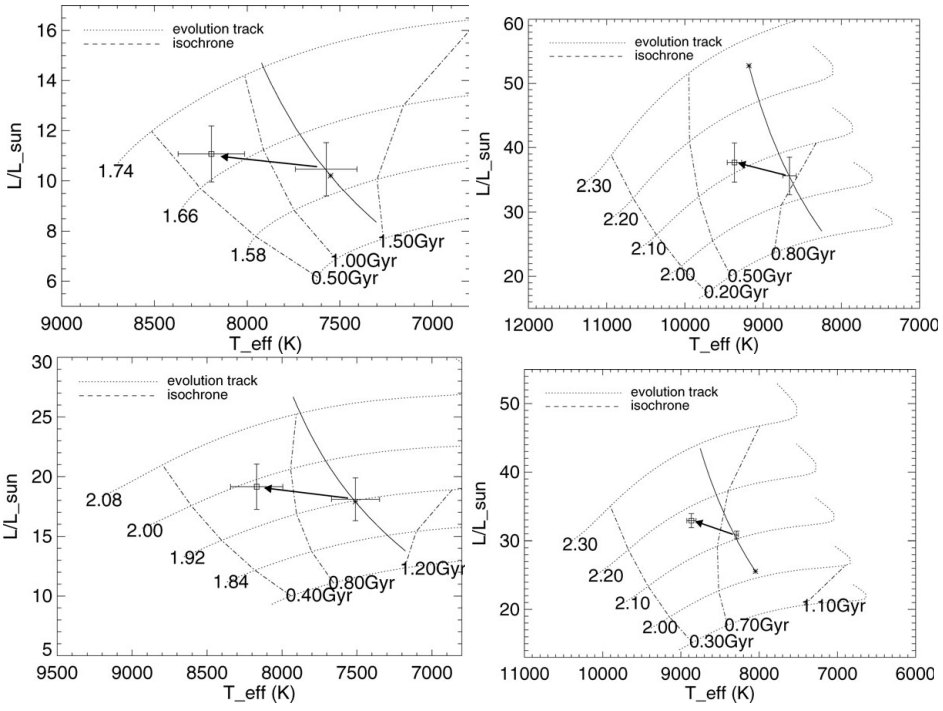

Figure 6. Locations of Altair (top left), Vega (top right), Alderamin (bottom left) and Rasalhague (bottom right) on the HR diagram. The Y^2 models (Demarque *et al.* 2004) are used to calculate the evolution tracks and the isochrones. The solid lines show the positions of each star on the H-R diagram as a function of inclination. The error bars across the inclination curves mark the true T_{eff}s and true luminosities of the stars, while the asterisks on the curves indicate their apparent T_{eff}s and luminosities which are dependent on their inclinations. Lastly, the squares with error bars in the left mark the non-rotating equivalent position for each star to allow comparison to the isochrones.

(bottom right panel), its apparent position is at the lower end of the curve; and for a 0^o inclination star such as Vega (top right panel), its apparent position is at the higher end of the curves. The inclination-dependent temperature and luminosity of rapid rotators can also bring scatters and errors to the HR diagram.

7. Conclusions and Future Prospects

We have presented and discussed the interferometric observations of seven rapid rotators studied to date, ranging from spectra type B3 to F2. These measurements and images have directly confirmed the basic picture of the standard model, but have also discovered discrepancies, suggesting more sophisticated mechanisms such as non-uniform rotation are necessary to be taken into account. Overall, these observations have greatly improved our knowledge of rapid rotators, demonstrating that optical interferometry is now mature to provide valuable constraints and even model-independent images to shed light on the basic physics of stars.

For the near future, multi-wavelength interferometric observations in both near-IR and visible are already on the horizon. Since gravity darkening is much more prominent at shorter wavelengths, observations with optical combiners such as CHARA-VEGA, CHARA-PAVO, and VLTI-MATISSE will be able to study stars in unprecedented details together with valuable spectral information. The current sample size will also be increased

toward fainter and smaller stars with higher angular resolution in shorter wavelengths. In addition, differential interferometry (Domiciano de Souza 2009) will also allow us to measure the differential rotation of rapid rotators and shed light on the issues of non-uniform rotation.

Interferometric observations can be even more valuable when combined with other techniques to provide multi-dimensional views of stars. The well determined geometry and rotational speed of a rapid rotator by interferometry can help to constrain models from other techniques. Such joint studies have already been applied in some spectroscopic studies (e.g., Yoon *et al.* 2008), and most recently, in asteroseimology studies as well (Monnier *et al.* 2010). More joint studies with interferometry and other techniques is a promising direction in the near future, and is expected to further advance our knowledges of the underlying physics of stellar rotation.

References

Abt, H. A., Levato, H., & Grosso, M. 2002, *ApJ*, 573, 359
Abt, H. A. & Morrell, N. I. 1995, *ApJS*, 99, 135
Aufdenberg, J. P., Mérand, A., Coudé du Foresto, V., Absil, O. *et al.* 2006, *ApJ*, 645, 664
Bohlin, R. C. & Gililand, R. L. 2004, *AJ*, 127, 3508
Burrows, A., Dessart, L., Livne, E., Ott, C. D. *et al.* 2007, *ApJ*, 664, 416
Claret, A. 2003, *A&A*, 406, 623
Cotton, W., Monnier, J., Baron, F., Hofmann, K.-H. *et al.* 2008, in: (eds.), *Society of Photo-Optical Instrumentation Engineers (SPIE) Conference Series* 7013
Cranmer, S. R. & Owocki, S. P. 1995, *ApJ*, 440, 308
Demarque, P., Woo, J.-H., Kim, Y.-C., & Yi, S. K. 2004, *ApJS*, 155, 667
Domiciano de Souza, A., Kervella, P., Jankov, S., Abe, L. *et al.* 2003, *A&A*, 407, L47
Domiciano de Souza, A., Kervella, P., Jankov, S., Vakili, F. *et al.* 2005, *A&A*, 442, 567
Domiciano de Souza, A. 2009, in: J.-P. Rozelot & C. Neiner (eds.), *The Rotation of Sun and Stars*, Lecture Notes in Physics 765 (Berlin Springer Verlag), p. 171
Frémat, Y., Zorec, J., Hubert, A.-M., & Floquet, M. 2005, *A&A*, 440, 305
Gies, D. R., Dieterich, S., Richardson, N. D., Riedel, A. R. *et al.* 2008, *ApJ* (Letters), 682, L117
Gizon, L. & Solanki, S. K. 2004, *Solar Phys.*, 220, 169
Gray, R. O., Corbally, C. J., Garrison, R. F., McFadden, M. T. *et al.* 2003, *AJ*, 126, 2048
Gray, R. O., Napier, M. G., & Winkler, L. I. 2001, *AJ*, 121, 2148
Gulliver, A. F., Hill, G. & Adelman, S. J. 1994, *ApJ* (Letters), 429, L81
Hill, G., Gulliver, A. F. & Adelman, S. J. 2004, in: J. Zverko, J. Ziznovsky, S. J. Adelman, & W. W. Weiss (eds.), *The A-Star Puzzle*, IAU Symposium 224, p. 35
Hill, G., Gulliver, A. F., & Adelman, S. J. 2010, *ApJ*, 712, 250
Högbom, J. A. 1974, *A&AS*, 15, 417
Ireland, M. J., Monnier, J. D., & Thureau, N. 2006, in: (eds.), *Society of Photo-Optical Instrumentation Engineers (SPIE) Conference Series* 6268
Jackson, S., MacGregor, K. B., & Skumanich, A. 2004, *ApJ*, 606, 1196
Jankov, S., Vakili, F., Domiciano de Souza, Jr., A., & Janot-Pacheco, E. 2001, *A&A*, 377, 721
Johnson, H. L. & Morgan, W. W. 1953, *ApJ*, 117, 313
Kanaan, S., Meilland, A., Stee, P., Zorec, J. *et al.* 2008, *A&A*, 486, 785
Kervella, P. & Domiciano de Souza, A. 2006, *A&A*, 453, 1059
Kurucz, R. L. 1993, VizieR Online Data Catalog, 6039
Lucy, L. B. 1967, *ZfA*, 65, 89
MacFadyen, A. I., Woosley, S. E., & Heger, A. 2001, *ApJ*, 550, 410
Maeder, A. & Meynet, G. 2000, *ARAA*, 38, 143
Maeder, A., Meynet, G., & Ekström, S. 2007, in: A. Vallenari, R. Tantalo, L. Portinari, & A. Moretti (eds.), *From Stars to Galaxies: Building the Pieces to Build Up the Universe*, ASP-CS 374, p. 13

MacGregor, K. B., Jackson, S., Skumanich, A., & Metcalfe, T. S. 2007, *ApJ*, 663, 560
Malbet, F., *et al.* 2010, in: W. C. Danchi, F. Delplancke & J. K. Rajagopal (eds.), *Optical and Infrared Interferometry*, SPIE Conference Series 7734, 138
Mason, B. D., Martin, C., Hartkopf, W. I., Barry, D. J. *et al.* 1999, *AJ*, 117, 1890
McAlister, H. A., ten Brummelaar, T. A., Gies, D. R., Huang, W. *et al.* 2005, *ApJ*, 628, 439
Millward, C. G. & Walker, G. A. H. 1985, *ApJS*, 57, 63
Monnier, J. D. 2003, *Reports on Progress in Physics*, 66, 789
Monnier, J. D., Berger, J.-P., Millan-Gabet, R., & ten Brummelaar, T. A. 2004, in: W. A. Traub (eds.), *New Frontiers in Stellar Interferometry*, SPIE Conference Series 5491, p. 1370
Monnier, J. D., Zhao, M., Pedretti, E., Thureau, N. *et al.* 2007, *Science*, 317, 342
Monnier, J. D., Townsend, R. H. D., Che, X., Zhao, M. *et al.* 2010, *ApJ*, 725, 1192
Narayan, R. & Nityananda, R. 1986, *ARAA*, 24, 127
Ohishi, N., Nordgren, T. E., & Hutter, D. J. 2004, *ApJ*, 612, 463
Petrov, R. G., Malbet, F., Weigelt, G., Antonelli, P. *et al.* 2007, *A&A*, 464, 1
Peterson, D. M., Hummel, C. A., Pauls, T. A., Armstrong, J. T. *et al.* 2006, *Nature*, 440, 896
Pinsonneault, M. 1997, *ARAA*, 35, 557
Rhee, J. H., Song, I., Zuckerman, B., & McElwain, M. 2007, *ApJ*, 660, 1556
Simon, T., Ayres, T. R., Redfield, S., & Linsky, J. L. 2002, *ApJ*, 579, 800
Thiébaut, E. 2008, in: M. Schöller, W. C. Danchi & F. Delplancke (eds.), *Optical and Infrared Interferometry*, SPIE Conference Series 7013, p. 43
Thompson, A. R., Moran, J. M., & Swenson, G. W. 1986, *Interferometry and synthesis in radio astronomy*, New York, Wiley-Interscience
van Belle, G. T., Ciardi, D. R., ten Brummelaar, T., McAlister, H. A. *et al.* 2006, *ApJ*, 637, 494
van Belle, G. T., Ciardi, D. R., Thompson, R. R., Akeson, R. L. *et al.* 2001, *ApJ*, 559, 1155
Vinicius, M. M. F., Zorec, J., Leister, N. V., & Levenhagen, R. S. 2006, *A&A*, 446, 643
von Zeipel, H. 1924a, *MNRAS*, 84, 665
von Zeipel, H. 1924b, *MNRAS*, 84, 684
Wagman, N. E. 1946, *AJ*, 52Q, 50
Walter, F. M., Matthews, L. D., & Linsky, J. L. 1995, *ApJ*, 447, 353
Yoon, J., Peterson, D. M., Zagarello, R. J., Armstrong, J. T. *et al.* 2008, *ApJ*, 681, 570
Zahn, J.-P., Ranc, C., & Morel, P. 2010, *A&A*, 517, A7+
Zhao, M., Gies, D., Monnier, J. D., Thureau, N. *et al.* 2008, *ApJ* (Letters), 684, L95
Zhao, M., Monnier, J. D., Pedretti, E., Thureau, N. *et al.* 2009, *ApJ*, 701, 209

Discussion

HUANG: I have a question on Regulus 2010 results. Is this imaging technique accurate enough to constrain the β value? There are several parameters entangled here, $v \sin i$, mass, β.

ZHAO: The β values are constrained by the gravity darkening models. Under the assumption of the Roche - von Zeipel law, they can be constrained pretty well as long as the stars are well resolved and not symmetric (i.e., not pole-on or equator on).

GIES: Observers use both critical velocity of Ω/Ω_{crit} and V_{eq}/V_{crit}. These will be different (reason Huang was concerned about the result for Regulus). And the one used here is the angular velocity.

TYCNER: Are the models you show fitted/constrainted by the reconstructed images or the actual data? If fitted/constrained by the data why not fitted/constrain by the image?

ZHAO: The models I showed are fitted by the actual data. It is always better to fit directly to the data than to the images. The images are not exact representations of the stars and, strictly speaking, they are also parameter-free models.